Université Jean Monnet
Mathematical Modelling Master Thesis

Performed at the Center for Biomedical and Healthcare Engineering of the
Ecole Nationale Supérieure des Mines de Saint-Étienne

Modelling, simulation and characterisation of human endothelial tessellations with Gaussian random fields

Patricio Guerrero
Directors: Yann Gavet, Jean-Charles Pinoli and Klervi Rannou

September, 2014

Acknowledgements

I would like to express my gratitude to the directors of this work, Yann Gavet and Jean-Charles Pinoli from the École Nationale Supérieure des Mines de Saint-Étienne, and to Klervi Rannou, the Ph.D. student who has specially collaborated and will continue working on this research.

I would also like to thank all my friends of the Center for Biomedical and Healthcare Engineering.

Contents

List of Figures

Introduction

This is a multidisciplinary work, covering theoretical fields such as probability theory, stochastic processes, geometry, topology, spatial statistics, mathematical morphology and image processing. The principal objective is to propose a new method to model, simulate and characterise two-dimensional random mosaics or tessellations. This new method is based on Gaussian random fields theory and on mathematical morphology techniques such as the watershed, the skeleton by influence zone among others.

The aim of obtaining two-dimensional mosaics is to develop a robust method to simulate human corneal endothelial tessellations close to identical endothelial images coming from optical microscopy (figure 1).

The cornea (figure 2) is the transparent part of the eyes in contact with the outside and its role is to refract the light toward the retina. The cornea is made of different layers, the epithelium in contact with the outside, the Descemet membrane, the stroma and the endothelium.

The human corneal endothelium is a monolayer of flat hexagonal cells, which do not regenerate and are responsible for the maintenance of the cornea transparency. During the first years of life, the human corneal endothelial mosaic is nearly a regular hexagonal tessellation. But with corneal growth and corneal diseases, the endothelial cells become less regular in shape and size. Ophthalmologists need to have more knowledge about the endothelium, and above all about the cell density and morphology, to control in a better way grafts and disease evolution.

The methodology proposed to simulated such tessellations basically consist on applying mathematical morphology techniques to simulated two-dimensional Gaussian random fields. This technique differs to usual ones that creates tessellation through Voronoi diagrams generated by a random point process. Such approach can be found in [9].

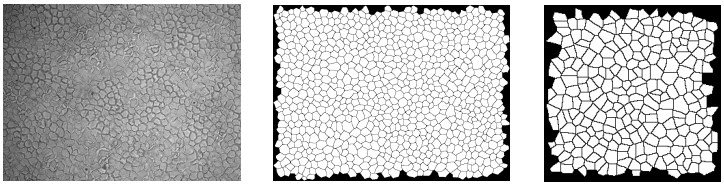

(a) Optic endothelial image

(b) Segmented endothelial image

(c) Simulated image

Figure 1: Real and simulated human corneal endothelial images.

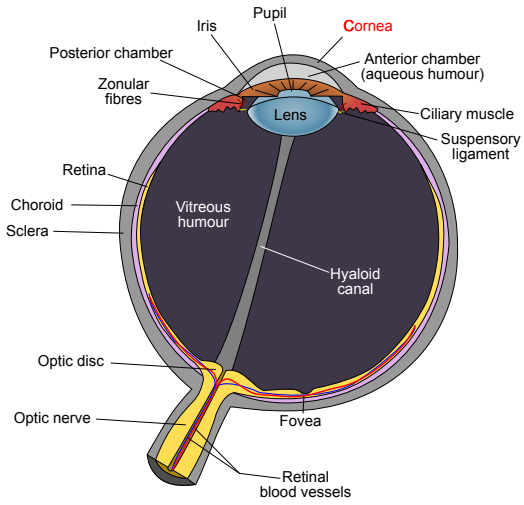

Figure 2: The human eye.

Context

The global project where this research belongs is the CNRS-ANR[1] Project CorImMo 3D: *Imagerie et Morphologie Microscopiques tri-dimensionnelles de l'endothélium cornéen humain* (Three-dimensional microscopic imaging and morphology of the human corneal endothelium). This project started in 2012 and the interest is the study and diagnostic of pathologies of the human endothelium. Here comes the necessity of modelling and simulation this monolayer to a better understanding of its behaviour.

This work was performed at the Center for Biomedical and Healthcare Engineering of the Ecole Nationale Supérieure des Mines de Saint-Étienne (UMR CNRS 5307).
Partnerships: BiiGC Biologie, Ingénierie et Imagerie de la Greffe de Cornée, and the society TRIBVN.

Organization of this document

First, basic concepts regarding random fields are presented in the first chapter, then, mathematical morphology techniques to create tessellations are presented in the second one. The third chapter study the characterization of these simulated tessellations, including morphometrical and granulometrical analysis. Finally, with a concluding chapter this research report is closed.

[1] CNRS: Centre national de la recherche scientifique. ANR: Agence nationale de la recherche.

Chapter 1

Random fields

In this chapter, necessary technical definitions about stochastic geometry are introduced. Particularly, Gaussian random fields are studied, as well as their geometrical characteristics, some covariance functions and their numerical simulation techniques.

Theory and applications of random fields have been developed in [3, 4]. Most important concepts and results are summarised in [1].

A *random field* is a stochastic process or a random function, taking values in a Euclidean space ($\mathbb{R}$ in this work, then it is called a *real-valued* random field), and defined over a parameter space. A formal definition follows.

Definition 1 *Let $(\Omega, \mathcal{F}, \mathbb{P})$ be a probability space and T a topological space. A real-valued random field X is given by*

$$\begin{aligned} X: \quad & T \times \Omega \longrightarrow \mathbb{R} \\ & (t, \omega) \longmapsto X(t, \omega) \end{aligned}$$

if for all $t \in T$ the map

$$\begin{aligned} X(t, .): \quad & \Omega \longrightarrow \mathbb{R} \\ & \omega \longmapsto X(t, \omega) \end{aligned}$$

is measurable.

For simplicity in notation, the dependency on the sample space Ω will be considered as implied and a random field $X(t, w)$ at location $t \in T$ will be simply noted as X_t in this work.

If the dimension of T is N, the associated random field is therefore called a $N-$dimensional random field. A one-dimensional random field is often called a *stochastic process*. In this work, we will work with two-dimensional random fields.

1.1 Gaussian random fields

Gaussian random fields have been used as models for many natural phenomena such as human brain mapping or galaxy density [21], they will be the principal tool to reach the objective of this work.

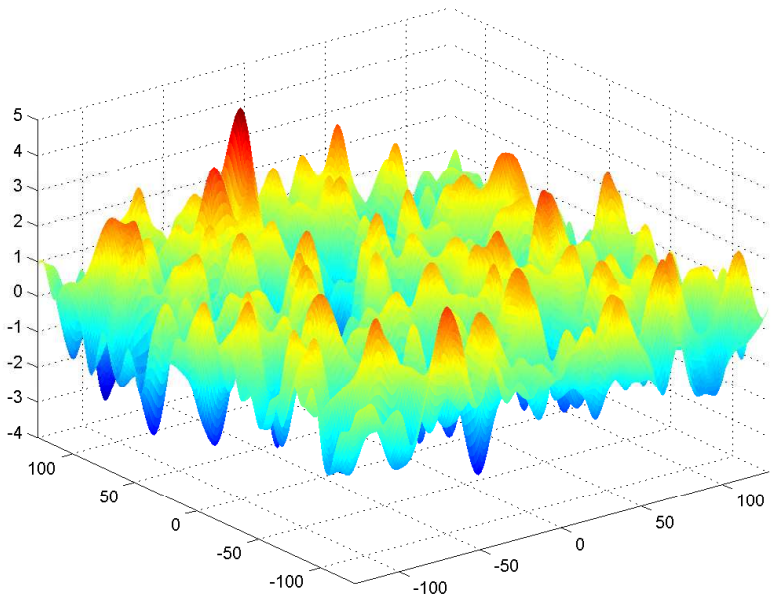

Figure 1.1: A two-dimensional real-valued Gaussian random field

Some preliminary basic definitions are introduced before defining formally a Gaussian random field [4].

A real-valued random variable $\hat{X}$ is said to be *Gaussian* if it has the density function:

$$\varphi(x) = \frac{1}{\sqrt{2\pi}\sigma} \exp\left(-\frac{(x-m)^2}{2\sigma^2}\right), \quad \forall x \in \mathbb{R}$$

where $m \in \mathbb{R}$ is the mean of $\hat{X}$ and $\sigma > 0$ its variance.

An $\mathbb{R}^k$-valued random variable $\tilde{X}$ is said to be *multivariate Gaussian* if for all $(\alpha_1, \ldots, \alpha_k) \in \mathbb{R}^k$, the real-valued variable $\sum_{i=1}^k \alpha_i \tilde{X}_i$ is Gaussian. In this case, the probability density is given by:

$$\varphi(x) = \frac{1}{(2\pi)^{\frac{d}{2}} \det(C)^{\frac{1}{2}}} \exp\left(-\frac{1}{2}(x-m)C^{-1}(x-m)'\right), \quad \forall x \in \mathbb{R}^k$$

where $m \in \mathbb{R}^k$ is the mean vector of $\tilde{X}$ ($m_j = \mathbb{E}\{\tilde{X}_j\}$), and C its covariance matrix, witch is a nonnegative definite $k \times k$ matrix, with elements $c_{ij} = \mathbb{E}\{(\tilde{X}_i - m_i)(\tilde{X}_j - m_j)\}$.

For notation purposes, we write that $\tilde{X} \sim \mathcal{N}(m, C)$ and $\hat{X} \sim \mathcal{N}(m, \sigma^2)$ for the one-dimensional case. The next definition introduces a real-valued Gaussian random field, in figure 1.1 a realisation of a two-dimensional one is exhibit.

Definition 2 *A real-valued Gaussian random field is a random field X such that for all $k \in \mathbb{N}^*$ and for all $(t_1, \cdots, t_k) \in T^k$, $(X_{t_1}, \cdots, X_{t_k})$ is multivariate Gaussian.*

Mean and covariance functions

Let (t, s) be in $T \times T$. The function:

$$m(t) = \mathbb{E}\{X_t\}$$

and the positive-definite[1] function:

$$C(t, s) = \mathrm{Cov}(X_t, X_s) = \mathbb{E}\{X_t X_s\} - \mathbb{E}\{X_t\}\mathbb{E}\{X_s\}$$

are called the *mean* and *covariance functions* of X, respectively.

The variance σ^2 of X is then defined as:

$$\sigma^2(t) = C(t, t)$$

A Gaussian random field is completely determined by the mean and covariance functions. In this work, we will be working with a particular class of Gaussian random fields, namely *stationary* and *isotropic* fields, defined in the next sections. The chose of the covariance function is a crucial aspect regarding the properties of the random field. No real structure is required of the parameter space T.

1.1.1 Symmetries

In this section, some important characteristics of Gaussian random fields are defined, they are introduced to understand the structure, geometrical and morphometrical properties of random fields.

Stationarity

Definition 3 *A Gaussian random field X is a stationary[2] Gaussian random field if its expectancy is constant:*

$$\forall t \in T, \quad \exists \mathsf{m} \in \mathbb{R}, \quad m(t) = \mathsf{m}$$

and if its covariance function depends only on the difference between two points of T,

$$\forall (t, s) \in T \times T, \quad \exists \mathsf{C} : \mathbb{R} \to \mathbb{R}, \quad C(t, s) = \mathsf{C}(t - s)$$

For stationary random fields, the corresponding covariance function is called *stationary covariance function*.

[1] The positive-definiteness is fundamental. It is proved in [1, p. 6] that the class of covariance functions coincide with the class of positive definite functions.

[2] The definition presented here is that of stationarity in *wide sense*, propriety presented in Gaussian random fields of this work. For the definition of stationarity in *strict sense* see [1, 5].

Isotropy

Metric property is assumed here for the topological space T. Let consider the dimension of T equal to N, and T equipped with the Euclidean distance d:

$$\forall (t,s) \in T \times T, \quad d(t,s) = \left(\sum_{i=1}^{N} (t_i - s_i)^2 \right)^{1/2}$$

Definition 4 *A stationary Gaussian random field X is said to be isotropic*[3] *if the covariance function depends only on the Euclidean metric between two points of T :*

$$\forall (t,s) \in T \times T, \quad C(t,s) = \mathsf{C}(d(t,s))$$

This definition implies that isotropic Gaussian random fields are translation and rotation invariant, they don't have a privileged direction.

For an isotropic random field, the corresponding covariance function is called *isotropic covariance function*. It is a subclass of stationary functions.

1.2 Some isotropic covariance functions

In this section, the two isotropic covariance functions chosen to simulate Gaussian random fields in this work are presented, namely, the *Gaussian and Bessel covariance*. They were chosen due to the smoothness they present. The first one is infinitely differentiable and the second one, who is parametrized by two positive scalars ν and l[4], increase it smoothness as ν does [1, 14]. This smoothness property will reflect homogeneity in simulated endothelial cells.

We remind that these isotropic covariance functions depends only on the Euclidean metric between two points of T, notated as $\tau = d(t,s)$.

1.2.1 Gaussian covariance function

The Gaussian covariance function[5] (figure 1.2) is given, for all $\tau \geq 0$, by:

$$\mathsf{C}(\tau) = \exp\left(-\frac{\tau^2}{2l^2} \right)$$

where $l \geq 0$ is the correlation length. This function is infinitely differentiable, this means that a Gaussian random field simulated through it has mean-square derivatives of all orders ([1, 14]), and is therefore very smooth.

[3] Another interesting propriety of Gaussian random fields is the *anisotropy*, who is defined in [1, 5].
[4] ν and l define the correlation length and the slope of the covariance function, respectively.
[5] also called the *squared-exponential covariance function*.

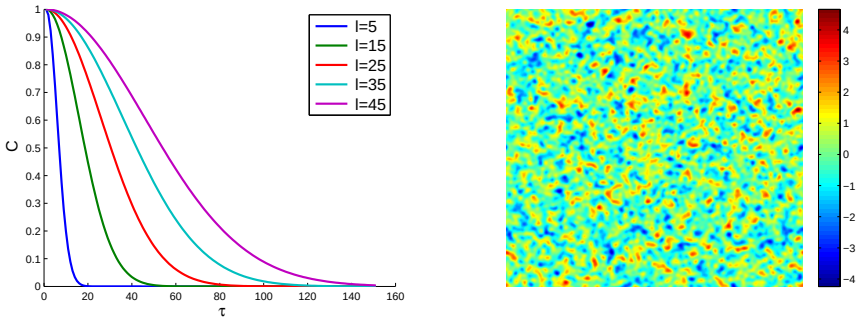

(a) Gaussian covariance function (b) Gaussian random field, $l = 5$

Figure 1.2: The Gaussian covariance function for different correlation lengths l. and a realisation of a Gaussian random field with a Gaussian covariance of correlation length $l = 5$.

1.2.2 Bessel covariance function of first kind

The Bessel covariance function (figure 1.3) is given, for all $\tau > 0$, by:

$$\mathsf{C}(\tau) = 2^{\nu}\Gamma(\nu+1)\left(\frac{\tau}{l}\right)^{-\nu} J_{\nu}\left(\frac{\tau}{l}\right)$$

where $\nu \geq \frac{N-2}{2}$ with N the dimensionality of T, Γ is the Gamma function and J_{ν} is the modified Bessel function of first kind of order ν given by:

$$\forall x \in \mathbb{R}^n, \quad J_{\nu}(x) = \left(\frac{x}{2}\right)^{\nu} \sum_{k=0}^{+\infty} \frac{(-1)^k}{\Gamma(k+1)\Gamma(\nu+k+1)} \left(\frac{x}{2}\right)^{2k}$$

The condition $\nu \geq \frac{N-2}{2}$ is necessary to verify the positive definiteness of the covariance function [22, p. 366]. The value $\frac{1}{l}$, often notes as ω describes the angular frequency of the function.

1.3 Simulation of Gaussian random fields

Regarding Gaussian random fields modelling and simulation, some theoretical definitions are needed, they come from [4, 5] and are presented here. Orthogonal expansions are the essential concept in simulating Gaussian processes. If T is a compact subset or $\mathbb{R}^N$ ($N = 2$ in this work), the *Karhunen-Loève expansion* is then used and, even more particularly, if the process is stationary, simulations are performed via the spectral representation approach using the Fourier transform.

1.3.1 Orthogonal and Karhunen-Loève expansions

Orthogonal expansions of Gaussian processes deal with simulating processes defined over a compact set of *any dimension*. The basic theory is presented here, and a simpler problem is studied regarding $N-$dimensional processes with the Karhunen-Loève expansion.

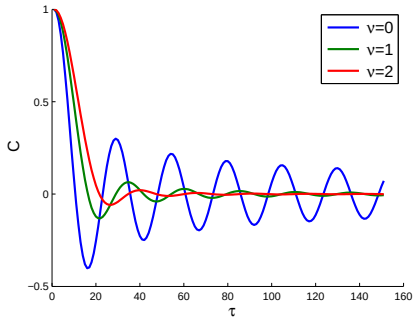

(a) Bessel covariance function

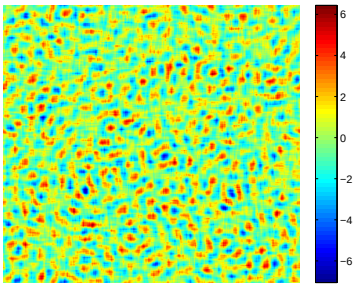

(b) Gaussian random field, $l = 4$, $\nu = 0$

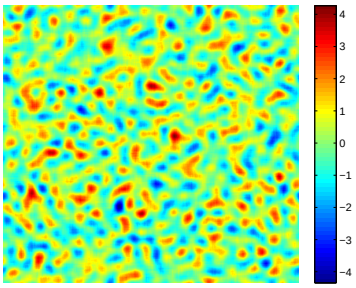

(c) Gaussian random field, $l = 4$, $\nu = 1$

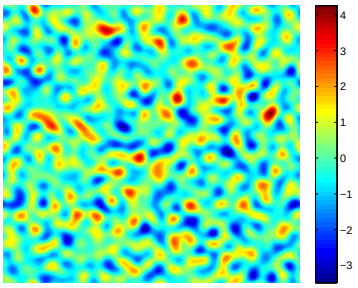

(d) Gaussian random field, $l = 4$, $\nu = 2$

Figure 1.3: The Bessel covariance function for different values of ν and for $l = 4$ (a), and realisations of Gaussian random fields with a Bessel covariance with different parameters (b)-(d).

The basic results of orthogonal expansion is established by theorem 1 [4, p. 69]:

Theorem 1 *Let X be a centred Gaussian random field with a continuous covariance function C, then it has an expansion of the form:*

$$X_t = \sum_{n=1}^{+\infty} \varphi_n(t)\xi_n$$

where $\{\xi_n\}$ are i.i.d[6] variables following a Gaussian distribution $\mathcal{N}(0,1)$ and $\{\varphi_n\}$ are functions defined on T depending on the covariance function C of X

The Karhunen-Loève expansion

Let $\lambda_1 \geq \lambda_2 \geq \ldots$, and $\psi_1, \psi_2, \ldots$, be the eigenvalues and normalized eigenfunctions, respectively, of the covariance function C of the Gaussian random field X. By definition, they solve the integral equation:

[6] independent, identically distributed

$$\int_T C(t,s)\psi(t)\mathrm{d}t = \lambda\psi(s), \tag{1.1}$$

With the normalisation:

$$\int_T \psi_n(t)\psi_m(t)\mathrm{d}t = \begin{cases} 1 & n = m \\ 0 & n \neq m \end{cases}$$

In the following, T will be considered as a compact subset of $\mathbb{R}^N$. The Karhunen-Loève expansion is a particular $N-$dimensional class of the orthogonal expansion of Gaussian processes. It is obtained by setting $\varphi_n = \sqrt{\lambda_n}\psi_n$ in the orthogonal expansion.

Consequently, the Karhunen-Loève expansion states that, under the same assumptions of theorem 1, X has an expansion of the form:

$$X_t = \sum_{n=1}^{+\infty} \sqrt{\lambda_n}\psi_n(t)\xi_n \tag{1.2}$$

These eigenfunctions mentioned above are the natural expansion of the covariance function C, according to Mercer's theorem[11].

Theorem 2 ***(Mercer)*** *Let C, λ_n, ψ_n and T be as above, then C has the expansion:*

$$C(t,s) = \sum_{n=1}^{+\infty} \lambda_n\psi_n(t)\psi_n(s) \quad \forall (t,s) \in T \times T$$

The Karhunen-Loève expansion leads to an eigenvalue problem that is not always easy to solve. As we work with stationary processes, this problem can be handled using the Fourier transform, detailed in the following section.

1.3.2 Spectral expansion

For a particularly class of random fields, the stationary ones, the simplest approach to generate them is using their spectral representation. Here, X is considered as a *complex-valued* random field, and the eigenfunctions ψ_n, solution of 1.1 can be easily established via complex exponentials. Namely, for any $\lambda \in \mathbb{R}^n$, the function: $t \mapsto e^{i<t,\lambda>}$ satisfies, with a change of variables $u = t - s$: ([4, p.73],[5, p.116])

$$\begin{aligned} \int_T C(t,s)e^{i<t,\lambda>}\mathrm{d}t &= \int_T \mathsf{C}(t-s)e^{i<t,\lambda>}\mathrm{d}t \\ &= e^{i<s,\lambda>}\int_T \mathsf{C}(u)e^{i<u,\lambda>}\mathrm{d}u \\ &= \tilde{\mathsf{C}}(\lambda)e^{i<s,\lambda>} \end{aligned}$$

where $\tilde{\mathsf{C}}(\lambda)$ is a possible zero scalar (is in fact the Fourier transform of C evaluated at λ).

Finally, the Karhunen-Loève expansion 1.2 becomes, if the number of $\tilde{\mathsf{C}}(\lambda)$ that are different to 0 is countable:

$$X_t = \sum_{\lambda} \sqrt{\tilde{\mathsf{C}}(\lambda)} e^{i<t,\lambda>} \xi_\lambda \tag{1.3}$$

where $\{\xi_\lambda\}$ are i.i.d complex-valued zero mean Gaussian variables[7]. Expression 1.3 corresponds to the inverse Fourier transform of the spectral coefficients $\sqrt{\tilde{\mathsf{C}}(\lambda)}\xi_\lambda$ evaluated at t.

For simulation purposes, the complex-valued Gaussian random field is discretized into a finite number of points belonging to T, therefore, the sum 1.3 is finite, and, in this work, only the real part of this random field is taken[8].

[7] A complex-valued random variable $\xi_1 + i\xi_2$ is said to be Gaussian if the vector of its two components (ξ_1, ξ_2) is bivariate Gaussian.

[8] Actually, we have two realisation of a real-valued Gaussian random field here considering the real and complex parts of this complex-valued Gausssian random field. If the complex part is taken, we would have another valid realisation of a real-valued Gaussian random field.

Chapter 2

Mathematical morphology

This chapter presents some basic tools provided by mathematical morphology and image processing. These concepts are used to simulate human endothelial tessellations from a Gaussian random field.

The theory of Gaussian random fields establishes properties of continuity and derivability of the processes, according to the properties of the covariance functions. However, for simulation purposes, the domain T of the Gaussian random field is discretized into a domain of size $2^n \times 2^n$ (pixels) where n changes according to the size we desire.

Consequently, in the following a simulated Gaussian random field is considered as a *grey-tone image* (it will be coloured with primary colours for clarity) defined over the integer grid $T = \{1, \ldots, 2^n\} \times \{1, \ldots, 2^n\}$ taking values in $\mathbb{R}$ and that their both univariate and multivariate distributions are all Gaussian. A realisation is illustrated in figure 2.1

2.1 Local maxima and $h-$maxima

The local maxima and $h-$maxima locations of a random field will be used as the generators or *markers* of the simulated tessellation and are introduced in this section. In the case of local maxima locations, they represent a set of points to create the associated *Voronoi*

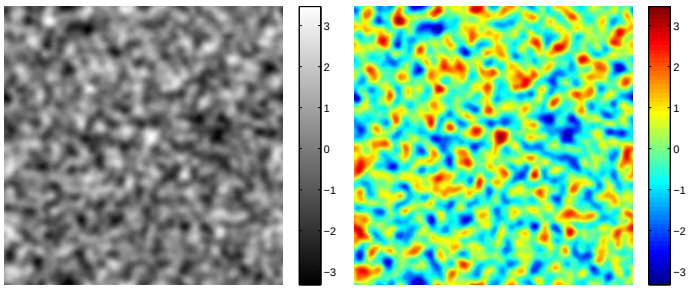

(a) Grey scale (b) Primary colour scale

Figure 2.1: A Gaussian random field considered as a grey-tone image (or an intensity image).

diagram, and for the $h-$maxima sets or *germs*, they are connected sets used to create the associated *skeleton by influence zone.*

All the concepts presented in this section belongs to morphological reconstruction operations, they are summarised in detail in [10, 20].

For a definition of *local maxima* or minima in terms of mathematical morphology, some preliminary concepts are needed. In the following, E is considered as an Euclidean space .

The *Minkowski addition* of two sets M and N belonging to E is formed by adding each vector in A to each vector in B and is denoted by $\oplus$:

$$M \oplus N = \{m+n | m \in M, n \in N\} = \bigcup_{m \in M,\, n \in N} \{m+n\}$$

Equivalently, the *Minkowski subtraction* $\ominus$ can be defined.

A *dilation* $\delta_S(M)$ of a set M by a set S of E (called structuring element) is defined as:

$$\delta_S(M) = M \oplus \check{S}$$

where $\check{S} = \{-s | s \in S\}$.

Finally, a *geodesic dilatation* $\delta_I(M)$ of a image M with respect to the image I is defined as:

$$\delta_I(M) = \inf\{\delta(M), I\}$$

where δ represents the *elementary dilation* (a dilation by a structuring element consisting in a pixel and its neighbours).

Local maxima

A local maximum M of a grey-tone image X (a simulated Gaussian random field in this work) at elevation r is a connected component of pixels with the value r whose external boundary pixels have a value strictly greater than r.

Definition 5 *M is a local maximum (resp. minimum) at level r if and only if M is connected and*

$$\begin{cases} \forall t \in M, & X_t = r, \\ \forall s \notin \delta(M) \setminus M, & X_s < r \ (\text{resp. } X_s > r). \end{cases}$$

The local maxima locations of a Gausian random field defined over T will be the generators of a Voronoi diagram (see section 2.2) that will represent a simulated endothelial tessellation.

Performing endothelial tessellations via Voronoi diagrams associated to local maxima locations of a Gaussian random field will create significantly small cells related to the mean cell size of the tessellation. This is due to some points that are too close to each other. The approach proposed to filter this irrelevant points is gathering them together through the $h-$maxima transform of a Gaussian random field.

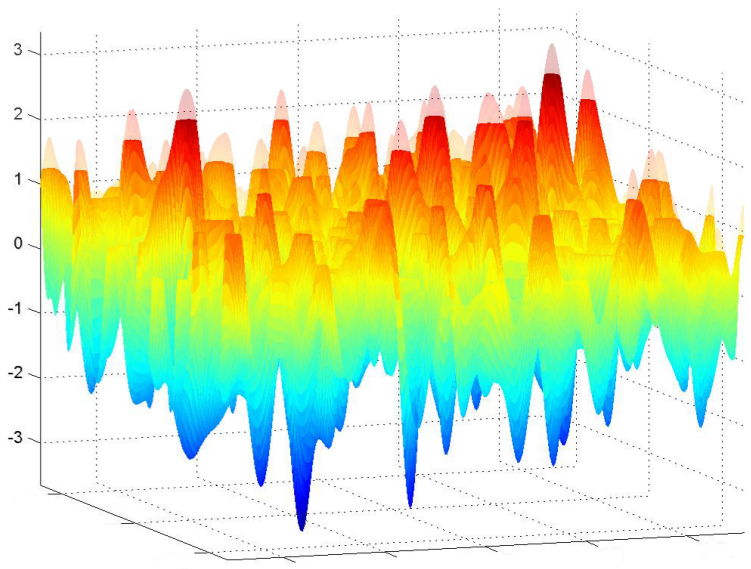

Figure 2.2: $h-$maxima transform of a Gaussian random field with $h = 0.5$, and in transparency the original field.

$h-$maxima

Let h be a positive real number. In order to filter irrelevant information about extrema of Gaussian random fields, the $h-$maxima transform suppresses all maxima whose depth is lower to h, it is defined by performing the geodesic dilation of $X - h$ with respect to X so many times until stability.

Formally, the $h-$maxima transform of a Gaussian random field X, illustrated in figure 2.2, can be defined as in [10]:

$$X^{(h)} = \lim_{n \to +\infty} \underbrace{\delta_X \circ \cdots \circ \delta_X}_{n \text{ times}}(X - h)$$

The *extended* $h-$maxima transform of a Gaussian random field X is defined as the local maxima of the corresponding $h-$maxima transform (Figures 2.4g and 2.4b). It is therefore a binary image assigning 1 to pixels belonging to local maxima of the $h-$maxima transform and 0 otherwise.

Definition of local and h maxima in terms of continuous paths

An interesting way to define a local maximum, an $h-$maximum and the link between them in terms of *paths* of a topographic surface is presented next, it can be found in [7]. We need first to define the concept of non-descending path and of a height of a path.

Definition 6 *Let X be a mean square continuous*[1] *and twice mean square derivable real-valued Gaussian random field and $[a,b] \subset \mathbb{R}$ an interval. A continuous path over X between two points s and t belonging to T : $\gamma_{s,t} : [a,b] \longrightarrow X$ such that $\gamma_{s,t}(a) = s$ and $\gamma_{s,t}(b) = t$, is a non-descending (resp. descending) path if for all $u, u' \in [a,b]$ such that $u < u'$, then $\gamma_{s,t}(u) \leq \gamma_{s,t}(u')$ (resp. $\gamma_{s,t}(u) \geq \gamma_{s,t}(u')$). The height of a non-descending or a descending path $\gamma_{s,t}$ is then:*

$$h(\gamma_{s,t}) = |X_t - X_s|$$

Next, we give a definition of a local maximum based on the non-descending paths and their height. This definition is useful to understand the link between a local maximum and an $h-$maximum.

Definition 7 *A point z of X belongs to a local maximum (resp. minimum) if and only if all non-descending (resp. descending) paths starting from z is of maximal height 0.*

Let h be a positive real number. A point z of X belongs to an $h-$maximum (resp. $h-$minimum) if and only if all non-descending (resp. descending) paths starting from z is of maximal height h.

2.2 Tessellations

A *tessellation* is the coverage of an open region with open, bounded and non-empty sub-regions with empty intersection. An example of a tessellation is the *Voronoi diagram*. A formal definition is given.

Definition 8 *Let $T \subseteq \mathbb{R}^N$, $N \geq 2$, be an open set. The set of open, bounded, non-empty and connected subsets $\{T_i\}_{i=1,\dots,k}$, $k \in \mathbb{N}^*$, is called a tessellation of T if and only if*

$$\forall i \in \{1,\dots,k\}, \quad \bar{T} = \cup_{i=1}^{k} \bar{T_i} \quad \text{and} \quad T_i \cap T_j = \emptyset, \quad \text{for} \quad i \neq j.$$

The aim is now to obtain tessellations from local maxima or $h-$maxima transforms of Gaussian random fields. Two ways to obtain such tessellations are presented: Voronoi diagrams and Skeletons by influence zone.

2.2.1 Voronoi diagrams

Voronoi diagrams create tessellations from a finite set of points, here, this set are the local maxima locations of a Gaussian random field. The Voronoi diagram, also named Dirichlet tessellation, has been introduced by Dirichlet in 1850, and generalised by Voronoi in 1908. For a good review about Voronoi diagrams, see [6]. In this section, T will be a bounded subset of $\mathbb{R}^2$.

[1] A random field X indexed by $T \subset \mathbb{R}^n$ is said to be mean square continuous if $\forall (t_n)_n \in T$ such that $d(t_n, t) \underset{n \to +\infty}{\longrightarrow} 0$, $\mathbb{E}\left[|X_{t_n} - X_t|^2\right]$ exists and converges to 0 when $n \to +\infty$.

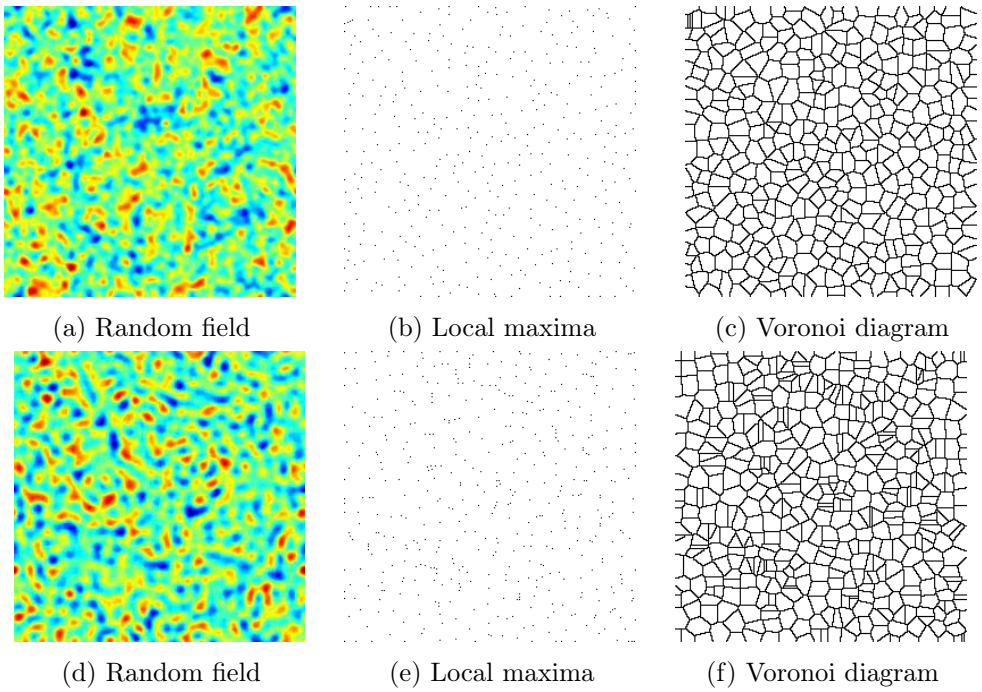

(a) Random field (b) Local maxima (c) Voronoi diagram

(d) Random field (e) Local maxima (f) Voronoi diagram

Figure 2.3: Simulation of endothelial tessellations through local maxima of a Gaussian random field. (a)-(c):With a Gaussian covariance. (d)-(f):With a Bessel covariance.

Definition 9 *Let $\mathcal{P} = \{p_1, \ldots, p_k\}$ be a finite set of points belonging to T and d a metric over the space T (usually the Euclidean metric). The Voronoi cell related to a point p_i is given by:*

$$Vor(p_i) = \{t \in T : \ d(t, p_i) < d(t, p_j), \ \forall p_j \in \mathcal{P}, j \neq i\}$$

and the Voronoi diagram associated to $\mathcal{P}$ is then:

$$Vor(\mathcal{P}) = T \cap \left(\bigcup_{i=1}^{k} Vor(p_i) \right)^c$$

Figure 2.3 illustrates the process of simulating tessellations from local maxima of Gaussian random fields via Voronoi diagrams created using the Euclidean metric. The points that are located close to each others are easily identifiable. The Voronoi diagram cannot be used with the $h-$maxima transform because they are compact and connected sets and not a set of points any longer. A similar tool than the Voronoi diagram is then needed to obtain a tessellation from such sets.

2.2.2 Skeleton by influence zone (SKIZ)

A generalisation named *skeleton by influence zone* or SKIZ (see mathematical details in [7]) of a Voronoi diagram is used when the generating points are compact and connected sets called *markers*.

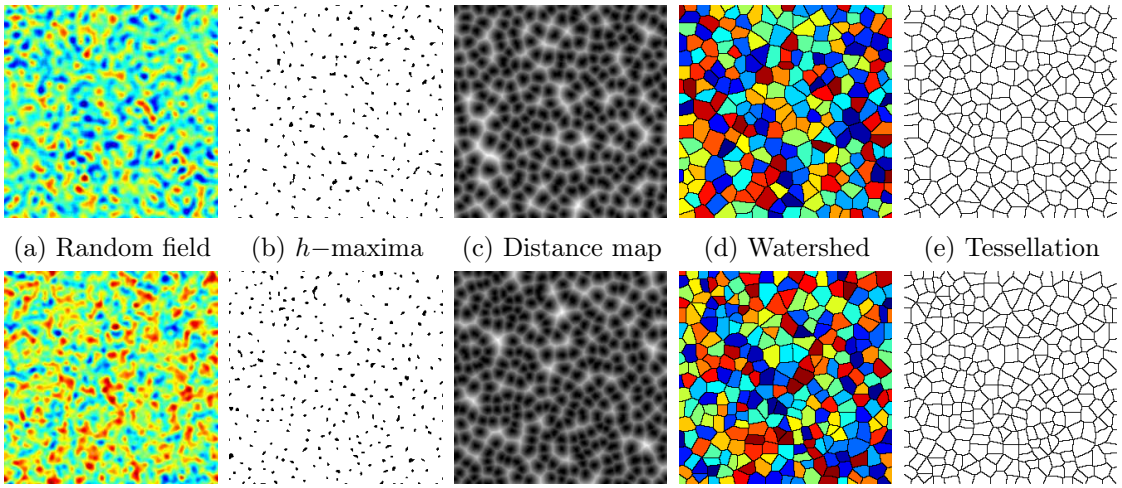

(a) Random field (b) $h-$maxima (c) Distance map (d) Watershed (e) Tessellation

(f) Random field (g) $h-$maxima (h) Distance map (i) Watershed (j) Tessellation

Figure 2.4: Simulation of endothelial tessellations through extended $h-$maxima of a Gaussian random field with $h = 0.2$. (a)-(e):With a Bessel covariance. (f)-(j):With a Gaussian covariance.

Definition 10 *Let $M = \{M_1, \ldots, M_k\} \subset T$ a set of markers. The influence zone* IZ *of a marker M_i is given by:*

$$\mathrm{IZ}(M_i) = \left\{ t \in T : \ d_{M_i}(t) < d_{M_j}(t), \ \forall M_j \in M, j \neq i \right\}$$

where for all set $A \subset T$:

$$\begin{aligned} d_A : \quad & T \longrightarrow \mathbb{R}^+ \\ & t \longmapsto \inf_{a \in A} d(a,t) \end{aligned}$$

is the distance transform related to the set A and d is the Euclidean metric in this work. The skeleton by influence zone of the set of markers M correspond to the boundaries of the influence zones of all the markers, namely:

$$\mathrm{SKIZ}(M) = T \setminus \left(\bigcup_{i=1}^{k} \mathrm{IZ}(M_i) \right)$$

2.2.3 Watershed

In mathematical morphology, the watershed transform, introduced in [7], is used in image segmentation for grey-scale images considered as topographical surface (figure 2.5). Here, it is applied on the distance map related to the $h-$maxima germs of the Gaussian random field to create tessellations.

The watershed transform is defined here over a topographical surface, because the concept of *topographical distances* is employed, defined as:

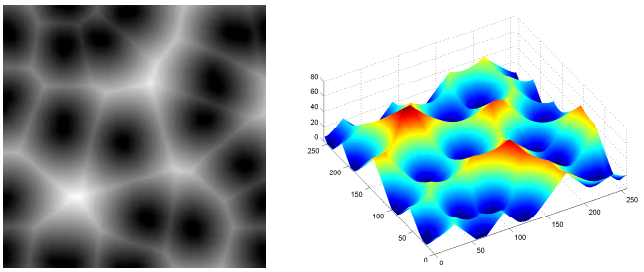

(a) Grey-tone image (b) Topographical surface

Figure 2.5: Topographical representation of a grey-tone image. Local minima in blue and the catchment basins can be appreciated. The watershed transform corresponds to the set of points that are in any catchment basin.

Definition 11 *Let S be a topographic surface given by a $\mathcal{C}^2$ function f. The topographic distance* TD_S *(see [12] and [13]) between two points p and q belonging to S is given by :*

$$\mathrm{TD}_S(p,q) = \inf_{\gamma \in \Gamma(p,q)} \int_\gamma \|\nabla f(\gamma(s))\| ds$$

where $\Gamma(p,q)$ is the set of paths between p and q. The topographic distance between a point $p \in S$ and a set $A \subset S$ is given by:

$$TD_f(p,A) = \min_{a \in A} TD_f(p,a)$$

The concept of *catchment basins* of a local minimum is also needed to define the watershed transform. Next, a definition of catchment basins and of the watershed transform.

Definition 12 *Let $\{m_i\}_{i=1,\cdots,k}$ be the minima's of the function f. The catchment basin* CB *of a minimum m_i is given by*

$$\mathrm{CB}(m_i) = \{t \in T : \forall j \neq i, \quad f(m_i) + TD_f(m_i,t) < f(m_j) + TD_f(m_j)\}$$

The watershed WS *of f is then the collections of points that are in the boundaries of the catchment basins of all local minima of f:*

$$\mathrm{WS}(f) = T \setminus \left(\bigcup_{i=1}^{k} \mathrm{CB}(m_i) \right)$$

SKIZ via the watershed transform

Numerically, the SKIZ can be generated by computing the watershed transform of the distance map (obtained by calculating the distance transform related to the $h-$maxima germs for each pixel of T, figures 2.4c and 2.4h) of the complement of the extended $h-$maxima of a Gaussian random field (considering that the extended $h-$maxima is a binary image),

and then looking for the *watershed* ridge lines (section 2.2.3) of the result. The process is illustrated in fig 2.4.

$$\mathrm{SKIZ}(M) = \mathrm{WS}(\delta_M(T)^c)$$

Criteria to characterize these tessellations and to compare them with segmented corneal mosaics are presented in the next chapter.

Chapter 3

Characterization

To determine whether our simulated tessellations are similar to human corneal mosaics, a characterization is made according to cell properties. A morphometric and a granulometric analysis are performed in the next sections.

3.1 Morphometry

3.1.1 Definitions

Shape diagrams, introduced in [8, 19] and developed in [15, 16, 17, 18], allow to represent compact sets according to their morphology. Representations are made by points in the domain $[0,1]^2$. Consequently, they provide an overview of the variability and distribution of shapes of compact sets. The coordinate axes of the points are morphometrical functionals defined as ratios of geometrical functionals of the considered sets. Most of the following definitions come from [18].

Geometrical functionals

In this section, human endothelial cells are considered as non-empty compact sets in the Euclidean 2D space $\mathbf{E}^2$. As in [18, 19], the studied geometrical functionals are the area, the perimeter, the radii of the inscribed and circumscribed circles, and the minimum and maximum Feret diameters[1] of the considered cells, denoted by A, P, r, R, w, d respectively.

These geometrical functionals verify geometrical inequalities [18] for compact sets. Such inequalities compare two geometrical functionals and determine the extremal compact set that satisfy the corresponding equality [3]. In this way, we can define the associated morphometrical functionals (Table 3.1).

[1] The minimum and maximum Feret diameters of a compact set are the minimal and the maximal orthogonal projections of the set on a line, respectively.

Table 3.1: Shape functionals for compact sets

Geometrical functionals	**Geometrical inequalities**	**morphometrical functionals**	**Extremal set**
w, d	$w \leq d$	w/d	constant width convex sets
A, d	$4A \leq \pi d^2$	$4A/\pi d^2$	disk
r, P	$2\pi r \leq P$	$2\pi r/P$	disk
R, P	$4R \leq P$	$4R/P$	line segment

Table 3.2: The two shape diagrams chosen

Shape diagram	$3-$tuplet dependency	$x-$**coordinate**	$y-$**coordinate**
$\mathcal{D}_1$	(w, A, d)	w/d	$4A/\pi d^2$
$\mathcal{D}_2$	(r, R, P)	$2\pi r/P$	$4R/P$

Morphometrical functionals

The morphometrical functionals are defined as ratios between geometrical functionals in order for its value to be 1 when its associated inequality becomes an equality, namely, the extremal set. They do not depend on the global size of the compact set, this is due to the fact that they have no unit. Their values range in $[0, 1]$. Finally, they are classified according their meanings, particularly:

$4A/\pi d^2$ corresponds to the roundness, $2\pi r/P$ to the circularity, w/d to the diameter constancy and $4R/P$ to its thinness.

Shape diagrams

For human endothelial cells, shape diagrams are analysed. They are cloud point representations of compact sets defined with a $3-$tuplet of geometrical functionals (g_1, g_2, g_3), or equivalently, with two morphometrical functionals (m_1, m_2) valued in $[0, 1]^2$.

Here, m_1 is a ratio defined with the geometrical inequality between g_1 and g_3, while m_2 between g_2 and g_3. Both m_1 and m_2 use the same geometrical functional as denominator.

A shape diagram $\mathcal{D}$ is therefore represented in the plane domain $[0, 1]^2$ where each endothelial cell of the studied tessellation is mapped onto a point (x, y), whose coordinate axes are m_1 and m_2. It allows to study the pleomorphism (shape variability) of the considered cells.

Mathematically, a shape diagram $\mathcal{D}$ is obtained from the following mapping.

$$\mathcal{D} : \left\{ \begin{array}{lcl} \mathcal{K}(\mathbf{E}^2) & \rightarrow & [0, 1]^2 \\ S & \mapsto & (x, y) \end{array} \right.$$

where $\mathcal{K}(\mathbf{E}^2)$ denotes the compact sets of $\mathbf{E}^2$.

The study is limited to two shape diagrams, $\mathcal{D}_1$ and $\mathcal{D}_2$ (chosen according to the results of [15, 16, 17]), who depend on the $3-$tuplets of geometrical functionals: (w, A, d) and (r, R, P) respectively, defined in table 3.2. A more complete list of shape diagrams is presented in [18].

Table 3.3: Morphometrical functionals for regular polygons

	w/d	$4A/\pi d^2$	$2\pi r/P$	$4R/P$
segment	0	0	0	1
triangle	$\sqrt{3}/2$	$\sqrt{3}/\pi$	$\sqrt{3}\pi/9$	$4\sqrt{3}/9$
square	$\sqrt{2}/2$	$2/\pi$	$\pi/4$	$\sqrt{2}/2$
pentagon	$\frac{1}{4}\tan\frac{2\pi}{5}\sec\frac{\pi}{5}$	$\frac{5}{4\pi}\sec\frac{\pi}{5}\csc\frac{\pi}{5}$	$\frac{\pi}{5}\cot\frac{\pi}{5}$	$\frac{2}{5}\csc\frac{\pi}{5}$
hexagon	$\sqrt{3}/2$	$3\sqrt{3}/2\pi$	$\sqrt{3}\pi/6$	$2/3$
disk	1	1	1	$2/\pi$

3.1.2 Endothelial images

For the two manually segmented endothelial tessellations showed in the previous section, each of their cells are numbered and mapped onto the diagrams $\mathcal{D}_1$ and $\mathcal{D}_2$ (figure 3.1). In accordance with the concept, cells with a remarkable difference in shape with respect to the others are mapped away from the others (red-colored) in the diagrams.

As reference, the Cartesian position of some regular polygons: the triangle, the square, the pentagon, the hexagon, the disk and the line segment are located in the presented diagrams. The values of their morphometrical functionals are analytically calculated (table 3.3).

3.1.3 Simulated images

For simulated images obtained from Gaussian random fields with Gaussian and Bessel covariance, the studied shape diagrams are presented (figure 3.2). Same number of cells are represented in each shape diagram studied.

To analyse the homogeneity of simulated cells, two statistical criteria are studied, the root-mean-squared distance (definition 13) of points in the diagram and the Euclidean distance between the centroids of the diagrams for simulated and for endothelial cells.

Root-mean-squared distance (RMSD)

The root-mean-squared distance characterize the amount of 2D dispersion of points around the centroid of the diagram. It's a scalar number that increase if the variability of points positions is more important, that is to say the RMSD gives an information of the shape homogeneity according to the diagrams.

Definition 13 *Let* $(\mathbf{x}, \mathbf{y}) = (x_1, y_1), \ldots, (x_N, y_N)$ *be* N *points in the* $\mathbb{R}^2$ *domain. The root-mean-squared distance of* $(\mathbf{x}, \mathbf{y})$ *is given by*

$$\mathrm{RMSD}(\mathbf{x}, \mathbf{y}) = \sqrt{\sigma_{\mathbf{x}}^2 + \sigma_{\mathbf{y}}^2}$$

Or equivalently, by

$$\mathrm{RMSD}(\mathbf{x}, \mathbf{y}) = \sqrt{\frac{1}{N-1}\sum_{i=1}^{N}((x_i - \bar{x})^2 + (y_i - \bar{y})^2)}$$

where $\sigma_{\mathbf{x}}$ *and* $\bar{x}$ *are the standard deviation and the mean of the vector* $\mathbf{x}$ *respectively.*

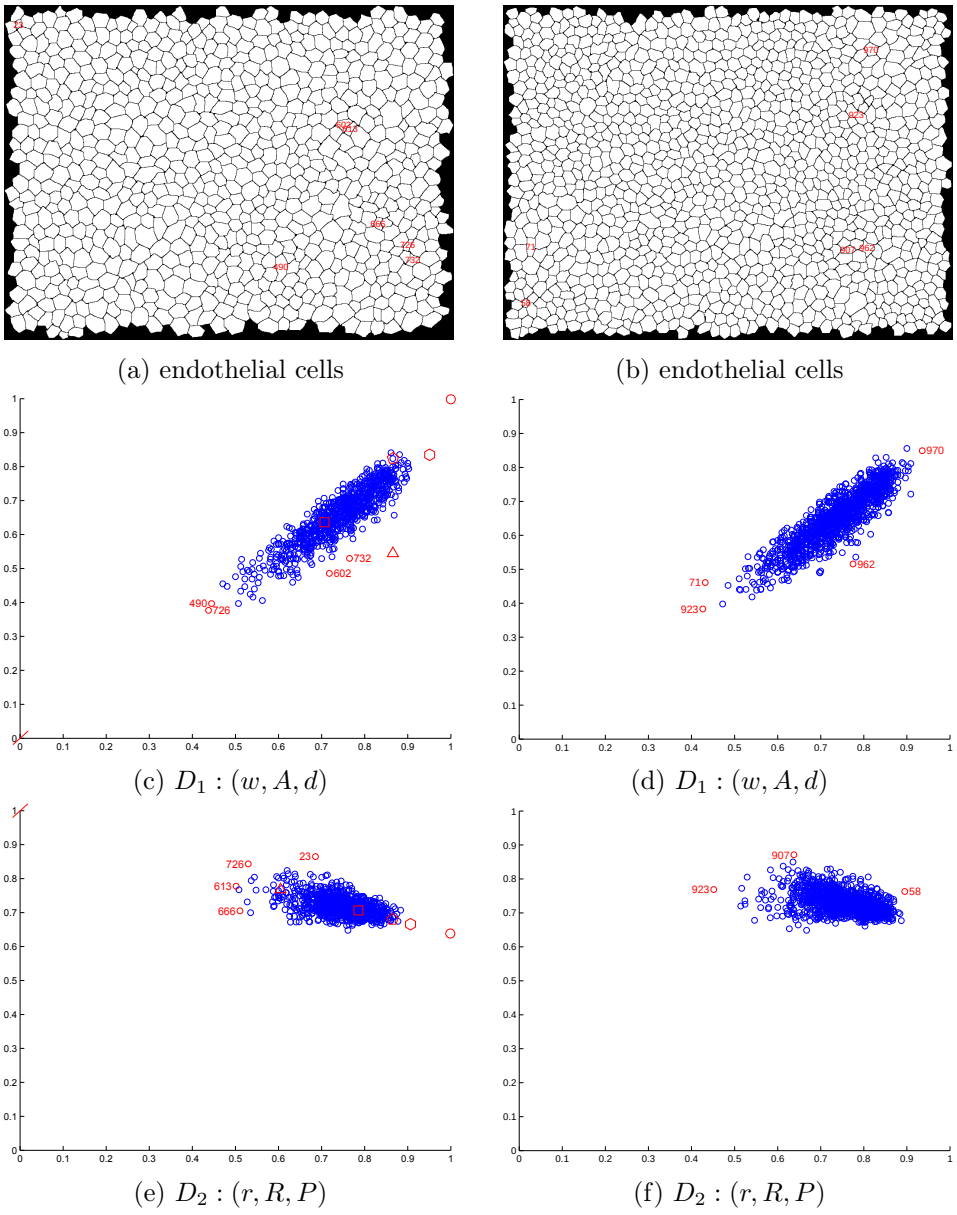

Figure 3.1: Shape diagrams D_1 and D_2 for two manually segmented endothelial images. Particular cells whose Cartesian positions are visually more distant from the diagram centre are colored in red and located in the endothelial images. They have clearly a particularl morphology with respect to the others. Cartesian position of the triangle, the square, the pentagon, the hexagon, the disk and the line segment are also located as reference.

Table 3.4: Root-mean-squared distance (RMSD) and distance between centroids of shape diagrams of endothelial and simulated cells (δ). Simulated cells are obtained from the $h-$maxima transform of Gaussian random fields with Bessel and Gaussian covariance with $h \in \{0, 0.1, 0.2, 0.3, 0.4\}$. Highlighted in bold the more interesting results.

h	Bessel covariance				Gaussian covariance			
	D_1		D_2		D_1		D_2	
	RMSD	δ	RMSD	δ	RMSD	δ	RMSD	δ
0	0.339	0.073	0.17	0.062	0.244	0.102	0.128	0.078
0.1	**0.182**	**0.04**	**0.095**	0.047	0.23	0.091	**0.119**	0.066
0.2	0.196	0.054	0.105	0.044	0.229	0.09	0.12	0.059
0.3	0.2	0.061	0.109	**0.041**	**0.227**	**0.083**	0.122	**0.053**
0.4	0.206	0.07	0.114	0.042	0.233	0.097	0.128	0.056

Distance between centroids of diagrams (δ) and results

For corneal endothelial cells, taken from 14 manually segmented optical images, the centroid of the diagrams D_1 and D_2 are located, and then the Euclidean distance between them and the centroids of the different simulated cell diagrams δ are calculated. The aim here is to identify the shape diagram of simulated cells whose centroid is closer to that of endothelial cells.

Results are presented in table 3.4, for cells obtained from simulations of Gaussian random fields with different parameters.

3.1.4 Conclusion

As a first conclusion, according to the distance δ between centroids of shape diagrams, simulated cells obtained from Gaussian random fields with a Bessel covariance are closer to endothelial cells regarding their morphometrical characteristics than cells simulated with a Gaussian covariance. In addition, with a Bessel covariance, simulated cells present also more homogeneity in shape, considering the root-mean-squared distance of shape diagrams.

Analysing the effect of h of the $h-$maxima transform in the simulations, results with $h > 0.3$ are no longer interesting for both covariance functions. Geometrical criteria in the next section is studied to confirm this results.

3.2 Granulometry

Ophthalmologists are interested not only in the pleomorphism of endothelial cells, they are also concerned in the polymegathism (size variability) of cells. Consequently, a statistical study of the subject is performed. To this purpose, the area and perimeter distribution of endothelial cells are studied and the results are compared to those related to simulated cells.

3.2.1 Endothelial images

In order to have a good reference sample to compare with the simulated cells, the area and perimeter of 14 manually segmented optical images are calculated. But they are not

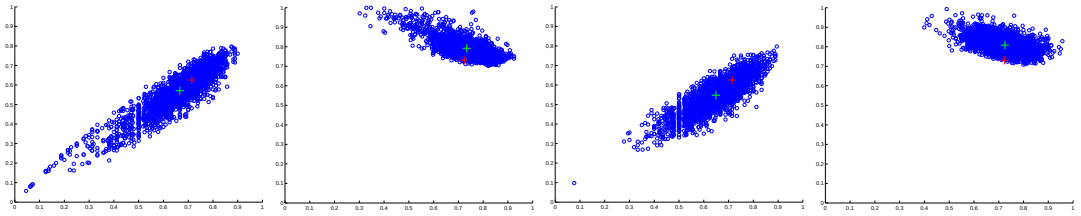

(a) D_1, local maxima $h = 0$ (b) D_2, local maxima $h = 0$ (c) D_1, local maxima $h = 0$ (d) D_2, local maxima $h = 0$

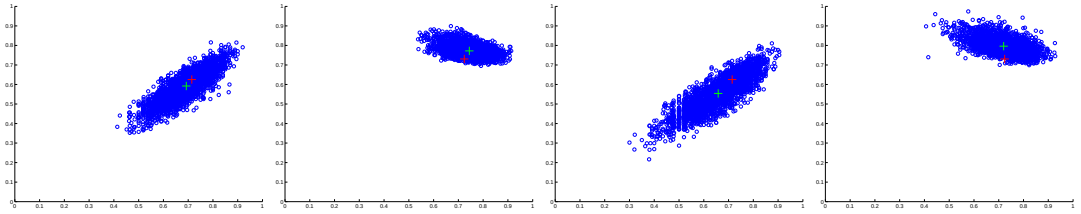

(e) D_1, $h-$maxima, $h = 0.1$ (f) D_2, $h-$maxima, $h = 0.1$ (g) D_1, $h-$maxima, $h = 0.1$ (h) D_2, $h-$maxima, $h = 0.1$

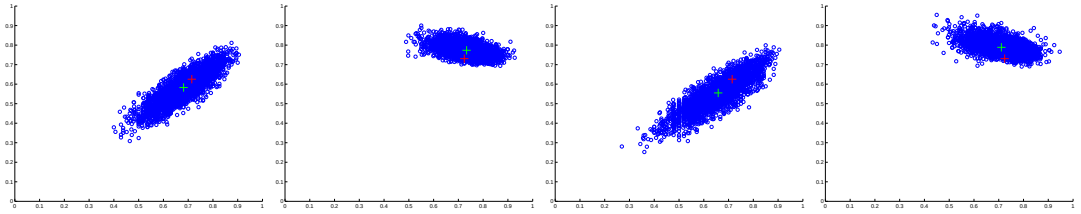

(i) D_1, $h-$maxima, $h = 0.2$ (j) D_2, $h-$maxima, $h = 0.2$ (k) D_1, $h-$maxima, $h = 0.2$ (l) D_2, $h-$maxima, $h = 0.2$

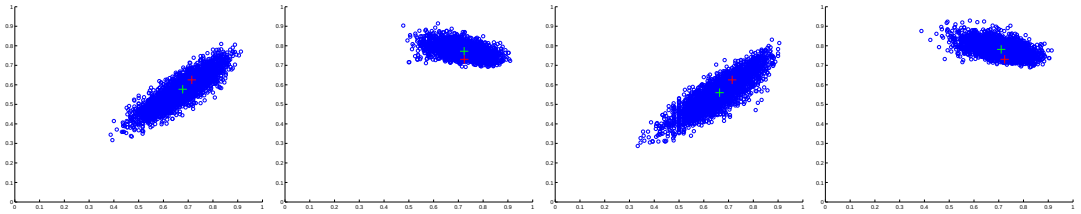

(m) D_1, $h-$maxima, $h = 0.3$ (n) D_2, $h-$maxima, $h = 0.3$ (o) D_1, $h-$maxima, $h = 0.3$ (p) D_2, $h-$maxima, $h = 0.3$

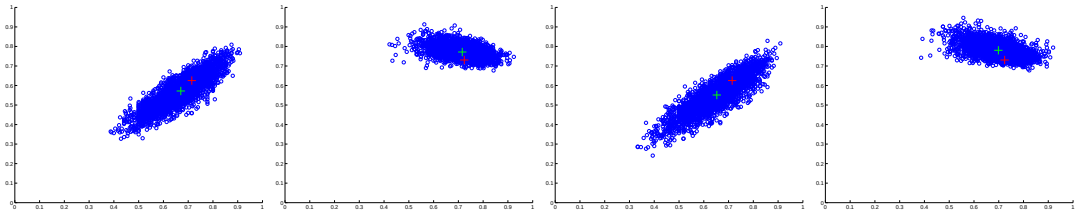

(q) D_1, $h-$maxima, $h = 0.4$ (r) D_2, $h-$maxima, $h = 0.4$ (s) D_1, $h-$maxima, $h = 0.4$ (t) D_2, $h-$maxima, $h = 0.4$

Figure 3.2: Effect of h in shape diagrams. Diagrams D_1 and D_2 for simulated cells with a Bessel covariance in the first and second columns respectively. The same for cells simulated with a Gaussian covariance in the two last columns. $+$: Centroid of diagram of endothelial cells presented as reference, $+$: centroid of the current diagram of simulated cells. 2760 cells represented in each diagram.

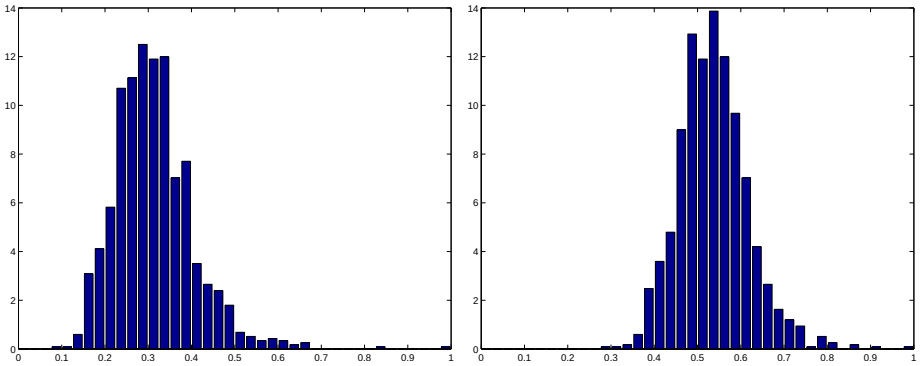

(a) Areas (b) Perimeters

Figure 3.3: Geometrical functionals of the endothelial image presenting the lowest CV of cell areas among 14 optical images. These distributions are the reference to be compared with simulated cells in the next section.

considered as a single vector, due to the different characteristics that each donor could present. Consequently, only one image will be chosen as reference, and this image is not chosen randomly. The coefficient of variation (CV) of corneal endothelial cell areas, defined as the ratio of the standard deviation to the mean of cell areas, is therefore used. CV is also used to analyse endothelial morphometry in [2].

To have the most homogeneous distribution in cell size, the lowest CV of endothelial cell areas is selected. This endothelial image has already been studied in previous sections (figure 3.1b), which CV value is 0.289. Maximum CV value is 0.445 and the mean is 0.346. Its area and perimeter distribution is presented in figure 3.3.

3.2.2 Simulated images

The simulated cells depend strictly on the choice of h in the $h-$maxima transform. For each h, the analysis is performed with about 5×10^5 simulated cells from Gaussian random fields (figure 3.4). Results confirm the interest of working with the extended $h-$maxima germs instead of the regional maxima points of the random field to create the tessellations. With the extended $h-$maxima germs, the number of significantly small cells in relation to the mean is reduced. This is in accordance with the spatial distribution and shape analysis of previous sections.

To compare area distributions, the Kolmogorov-Smirnof and the Wilcoxon-Mann-Whitney nonparametric tests are used. Kolmogorov-Smirnov ks statistic and Wilcoxon-Mann-Whitney z statistic are calculated between area distributions. Results are presented in table 3.5, and suggest again that tessellations obtained from Gaussian random fields with a Bessel covariance are closer to a human corneal endothelium with a value of h between 0.1 and 0.2.

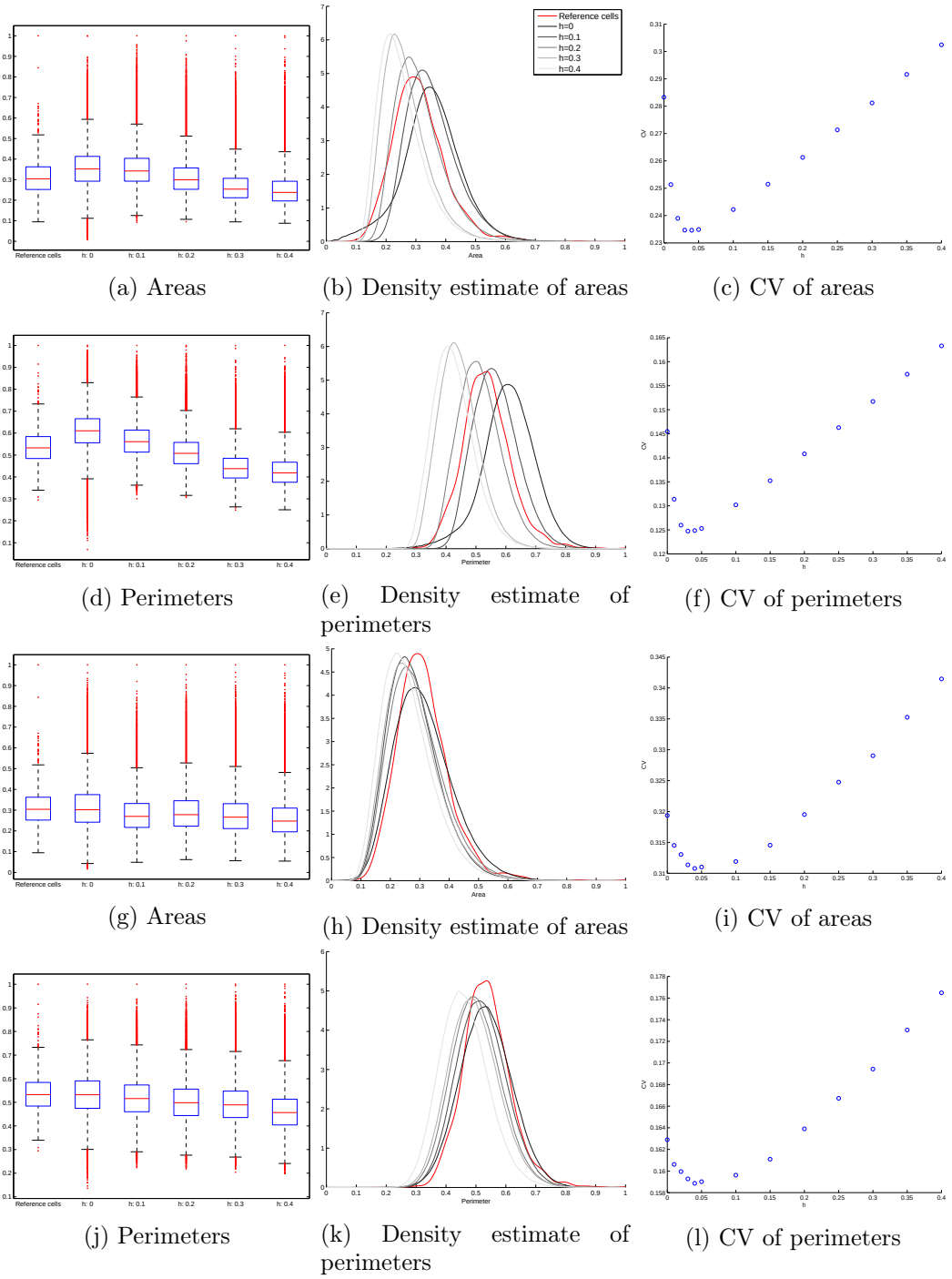

(a) Areas (b) Density estimate of areas (c) CV of areas

(d) Perimeters (e) Density estimate of perimeters (f) CV of perimeters

(g) Areas (h) Density estimate of areas (i) CV of areas

(j) Perimeters (k) Density estimate of perimeters (l) CV of perimeters

Figure 3.4: Effect of h in geometrical functionals. Cells obtained from Gaussian random fields with: (a)-(f): Bessel covariance. (g)-(l): Gaussian covariance. $h = 0$ corresponds to local maxima of a random field.

Table 3.5: Kolmogorov-Smirnov ks statistic and Wilcoxon-Mann-Whitney z statistic. Simulated cells are obtained from the $h-$maxima transform of Gaussian random fields with Bessel and Gaussian covariance with $h \in \{0, 0.1, 0.2, 0.3, 0.4\}$. Highlighted in bold the more interesting results.

h	Bessel covariance		Gaussian covariance	
	ks	z	ks	z
0	0.242	-16.534	**0.058**	**0.098**
0.1	0.209	-16.933	0.177	13.073
0.2	**0.039**	**0.279**	0.138	9.173
0.3	0.26	19.693	0.195	14.015
0.4	0.336	25.397	0.28	21.007

Chapter 4

Concluding discussion and perspectives

Random fields is a very exhaustive (interesting and useful in many applications) domain. In this work, some alternatives and variations of them are studied, nevertheless, perspectives are infinite. We worked mainly with Gaussian random fields, we therefore propose as alternative working with non-Gaussian random fields, or even with Gaussian-related random fields ($t-$*student, chi-squared*, etc.).

We also worked with the $h-$maxima transform regarding mathematical morphology, there are many others tools in this field that could be interesting to look at, namely the *top-hat*, global and local thresholding, etc.

Regarding the characterisation of cells, criteria about shape diagrams were introduced, a perspective work to compare two shape diagrams is considering a distance between them like the Hausdorff or the Fréchet distance.

Results and more perspectives

Random simulated human corneal endothelial tessellations presents satisfactory morphometrical and granulometrical properties. Usual techniques consists on Voronoi diagrams created from random points processes, such as *centroidal Voronoi tessellation* or *latin hypercube sampling*. The originality of this work consists in creating such diagrams not from a point process, but from a set of compact connected sets or *germs* obtained from a function as generators of the diagram who is then called skeleton by influence zone. These germs are obtained from the $h-$maxima transform of a Gaussian random field and a fundamental step of this method is to find an optimal value for this h.

We have locate an optimal interval, between 0.1 and 0.3 and an analytic analysis is now been researched to precise, if it exist, an optimal value for h.

Spatial repartition of local maxima of a Gaussian random field is a not developed area in this days. It is therefore motivating to continue working in probability theory regarding random fields, their geometrical properties and their extrema repartition.

The project CorImMo 3D is also interested in modelling three-dimensional images of the human corneal endothelium, a generalisation of the method presented in this work is

therefore proposed as a perspective.

Finally, we will submit a paper in *SIAM Journal on Imaging Sciences* presenting this work and results. The title of the paper is: *Modeling, simulation and characterisation of 2D spatial mosaics by means of random fields*. It will be submitted in October 2014.

Bibliography

[1] P. Abrahamsen. *A review of Gaussian random fields and correlation functions.* Norsk Regnesentral/Norwegian Computing Center, 1997.

[2] S. Acquart, P. Gain, M. Zhao, Y. Gavet, A. Defreyn, S. Piselli, O. Garraud, and G. Thuret. Endothelial Morphometry by Image Analysis of Corneas Organ Cultured at 31 degrees C. *Investigative Ophthalmology and Visual Science*, 51(3):1356–1364, March 2010.

[3] R. J. Adler. *The geometry of random fields.* Siam, 1981.

[4] R. J. Adler and J. E. Taylor. *Random fields and geometry.* Springer, 2007.

[5] O. Ahmad. *Stochastic representation and analysis of rough surface topography by random fields and integral geometry.* PhD thesis, École Nationale Supérieure des Mines de Saint-Étienne, 2013.

[6] F. Aurenhammer and R. Klein. Voronoi diagrams. *Handb. Comput. Geom.*, 5:201–290, 2000.

[7] S. Beucher and C. Lantuejoul. Use of watersheds in contour detection. 1979.

[8] W. Blaschke. Konvexe bereiche gegebener konstanter breite und kleinsten inhalts. *Math. Ann.*, 76(4):504–513, 1915.

[9] C. Bucht, P. Söderberg, and G. Manneberg. Simulation of specular microscopy images of corneal endothelium, a tool for control of measurement errors. *Acta ophthalmologica*, 89(3):e242–e250, 2011.

[10] Y. Gavet. *Perception visuelle humaine, complétion des mosaïques et application à la reconstruction d'images de l'endothélium cornéen humain en microscopie optique spéculaire.* PhD thesis, École Nationale Supérieure des Mines de Saint-Étienne, 2008.

[11] J. Mercer. Functions of positive and negative type and their connection with the theory of integral equations. *Philos. Trans. Roy. Soc. London*, pages 415–446, 1909.

[12] F. Meyer. Topographic distance and watershed lines. *Signal Process.*, 38(1):113–125, 1994.

[13] Laurent Najman and Michel Schmitt. Watershed of a continuous function. *Signal Processing*, 38(1):99–112, 1994.

[14] C. E. Rasmussen. Gaussian processes for machine learning. MIT Press, 2006.

[15] S. Rivollier, J. Debayle, and J.-C. Pinoli. Shape diagrams for 2d compact sets-part i: analytic convex sets. *Aust. J. Math. Anal. Appl.*, 7(2), 2010.

[16] S. Rivollier, J. Debayle, and J.-C. Pinoli. Shape diagrams for 2d compact sets-part ii: analytic simply connected sets. *Aust. J. Math. Anal. Appl.*, 7(2), 2010.

[17] S. Rivollier, J. Debayle, and J.-C. Pinoli. Shape diagrams for 2d compact sets-part iii: convexity discrimination for analytic and discretized simply connected sets. *Aust. J. Math. Anal. Appl.*, 7(2), 2010.

[18] S. Rivollier, J. Debayle, and J.-C. Pinoli. Shape representation and analysis of 2d compact sets by shape diagrams. In *Image Processing Theory Tools and Applications (IPTA), 2010 2nd International Conference on*, pages 411–416. IEEE, 2010.

[19] L. Santaló. Sobre los sistemas completos de desigualdades entre tres elementos de una figura convexa plana. *Math. Notae*, 17:82–104, 1961.

[20] P. Soille. *Morphological image analysis: principles and applications*. Springer, 2003.

[21] K. J. Worsley. The geometry of random images. *Chance*, 9(1):27–40, 1996.

[22] A. M. Yaglom. *Correlation theory of stationary and related random functions*. Springer, 1987.